cross points in a very straightforward, low-cost, fast, and scalable process. Although the separations between individual NWs are not completely uniform, a periodic array can be easily envisioned with a patterned surface as described above. These crossbar structures can yield functional devices (see below).

We believe that our approach for directed assembly of multiple crossed NW arrays offers substantial advantages over current efforts, which have used random deposition (*14*, *16*), direct manipulation of individual NWs and NTs (*15*), and electric fields (*12*, *16*, *27*) to make single crossed structures. With random deposition and manipulation, it is difficult to obtain multiple crossbars required for integrated nanodevices. Although electric fields enable more control over assembly, this method is also limited by (i) electrostatic interference between nearby electrodes as separations are scaled below the micrometer level and (ii) the requirement of extensive lithography to fabricate the electrodes for assembly of multiple NW device structures. Our fluidic approach is intrinsically very parallel and scalable and, moreover, it allows for the directed assembly of geometrically complex structures by simply controlling the angles between flow directions in sequential assembly steps. For example, an equilateral triangle (Fig. 4C) was assembled in a three-layer deposition sequence with 60° angles between the three flow directions. The method of flow alignment thus provides a flexible way to meet the requirements of many device configurations, including those requiring assembly of multiple "layers" of NWs.

An important feature of this layer-by-layer assembly scheme is that each layer is independent of the others, and thus a variety of homo- and heterojunction configurations can be obtained at each crossed point by simply changing the composition of the NW suspension used for each step. For example, it should be possible to directly assemble and subsequently address individual nanoscale devices using our approach with n-type and p-type NWs (*16*, *19*) and NTs, in which the NWs and NTs act as both the wiring and active device elements (*15*). A typical 2 by 2 crossbar array made of n-type InP NWs, in which all eight ends of the NWs are connected by metal electrodes, demonstrates this point (Fig. 4D). Transport measurements (Fig. 4E) show that current can flow through any two of the eight ends and enable the electrical characteristics of individual NWs and the NW-NW junctions to be assessed. The current-voltage (*I-V*) data recorded for each of the four cross points exhibit linear or nearly linear behavior (red curves) and are consistent with expectations for n-n type junctions. Because single NW-NW p-n junctions formed by random deposition exhibit behavior characteristic of light-emitting diodes (LEDs) (*16*), we believe that our approach could be used to assemble high-density and individually addressable nanoLEDs and electronically more complex nanodevices.

These studies provide a general and rational approach for hierarchical assembly of 1D nanomaterials into well-defined functional networks that can bridge the nanometer through millimeter size regimes. We have shown that NWs can be assembled into parallel arrays with control of the average separation and, by combining fluidic alignment with surface-patterning techniques, that it is also possible to control periodicity. In addition, we have demonstrated the possibility of layer-by-layer assembly of crossed and more complex structures by varying the flow direction in sequential steps and have obtained preliminary results suggesting that this approach can be extended to 1D nanostructures, such as carbon NTs (*28*). We believe that flow assembly represents a general strategy for organization of NW and NT building blocks into structures needed for wiring, interconnects, and functional devices and thus could enable a bottom-up manufacturing paradigm for future nanotechnologies.

References and Notes

1. J. Hu, T. W. Odom, C. M. Lieber, *Acc. Chem. Res.* **32**, 435 (1999).
2. C. Dekker, *Phys. Today* **52** (no. 5), 22 (1999).
3. J. R. Heath *et al.*, *Science* **280**, 1716 (1998).
4. C. A. Mirkin, *Inorg. Chem.* **39**, 2258 (2000).
5. C. B. Murray, C. R. Kagan, M. G. Bawendi, *Science* **270**, 1335 (1995).
6. C. P. Collier *et al.*, *Annu. Rev. Phys. Chem.* **49**, 371 (1998).
7. A. K. Boal *et al.*, *Nature* **404**, 746 (2000).
8. R. C. Hayward, D. A. Sayille, I. A. Aksay, *Nature* **404**, 56 (2000).
9. M. Li, H. Schnablegger, S. Mann, *Nature* **402**, 393 (1999).
10. J. Liu *et al.*, *Chem. Phys. Lett.* **303**, 125 (1999).
11. M. Burghard *et al.*, *Adv. Mater.* **10**, 584 (1998).
12. P. A. Smith *et al.*, *Appl. Phys. Lett.* **77**, 1399 (2000).
13. S. J. Tan *et al.*, *Nature* **393**, 49 (1998).
14. M. S. Fuher *et al.*, *Science* **288**, 494 (2000).
15. T. Rueckes *et al.*, *Science* **289**, 94 (2000).
16. X. Duan *et al.*, *Nature* **409**, 66 (2001).
17. S. Noda *et al.*, *Science* **289**, 604 (2000).
18. X. Duan, C. M. Lieber, *Adv. Mater.* **12**, 298 (2000).
19. Y. Cui, X. Duan, J. Hu, C. M. Lieber, *J. Phys. Chem. B* **104**, 5213 (2000).
20. D. C. Duffy *et al.*, *Anal. Chem.* **70**, 4974 (1998).
21. C. A. Stover, D. L. Koch, C. Cohen, *J. Fluid Mech.* **238**, 277 (1992).
22. D. L. Koch, E. S. G. Shaqfeh, *Phys. Fluids A* **2**, 2093 (1990).
23. We have shown that the NWs with well-defined and controllable lengths can be prepared using gold nanocluster catalysts (M. S. Gudiksen, J. Wang, C. M. Lieber, in preparation).
24. Y. Huang, X. Duan, C. M. Lieber, unpublished data.
25. C. De Rosa *et al.*, *Macromolecules* **33**, 4871 (2000).
26. M. Gleiche, L. F. Chi, H. Fuchs, *Nature* **403**, 173 (2000).
27. Electric fields can be used to align suspensions of semiconductor NWs into parallel NW arrays and single NW crosses (*16*), where patterned microelectrode arrays are used to create a field pattern. Fringing fields and charging can, however, lead to substantial complications in the assembly of multiple crosses at the submicrometer scale.
28. Additional studies show that suspensions of single-walled carbon nanotubes and duplex DNA can be aligned in parallel arrays with the fluidic approach.

29. We thank H. Stone, J. Ng, and T. Rueckes for helpful discussions. C.M.L. acknowledges support of this work by the Office of Naval Research and Defense Advanced Projects Research Agency.

10 October 2000; accepted 13 December 2000

Fast Drop Movements Resulting from the Phase Change on a Gradient Surface

Susan Daniel, Manoj K. Chaudhury,* John C. Chen

The movement of liquid drops on a surface with a radial surface tension gradient is described here. When saturated steam passes over a colder hydrophobic substrate, numerous water droplets nucleate and grow by coalescence with the surrounding drops. The merging droplets exhibit two-dimensional random motion somewhat like the Brownian movements of colloidal particles. When a surface tension gradient is designed into the substrate surface, the random movements of droplets are biased toward the more wettable side of the surface. Powered by the energies of coalescence and collimated by the forces of the chemical gradient, small drops (0.1 to 0.3 millimeter) display speeds that are hundreds to thousands of times faster than those of typical Marangoni flows. This effect has implications for passively enhancing heat transfer in heat exchangers and heat pipes.

The movements of liquids resulting from unbalanced surface tension forces constitute an important surface phenomenon, known as the Marangoni effect (*1*). When regulated properly, these types of flows are of value in several industrial applications, such as the design and operation of microfluidic and integrated DNA analysis devices (*2–4*). Although the usual Marangoni motions are triggered by variations in temperature or composition on a liquid surface, a surface tension heterogeneity (*5–7*) on a solid substrate can also induce such motion. The typical speeds of these flows (speeds ranging from micrometers to millimeters per second) on a

solid surface are too slow to have practical utility.

The main obstacle to drop motion on a solid surface arises from the hysteresis of contact angles that pin the drop edge. In order to surmount hysteresis, additional energy must be supplied to the drop while using the force arising from the gradient of surface tension to bias the drop motion. Here we report a new type of surface tension–guided flow, in which the drops move hundreds to thousand of times faster than the speeds of typical Marangoni flows. Furthermore, the experimental configurations used here provide a direct indication of how this effect can be harnessed to design improved heat exchangers. The central theme of these studies is that of rapid phase change, coupled with the fast removal of heat from steam condensing on a gradient surface.

The test surface for this study had a radially outward gradient of chemical composition that was prepared by diffusion-controlled silanization (*8*). A small drop (~2 μl) of alkyltrichlorosilane [$Cl_3Si(CH_2)_nCH_3$, n = 8 to 14] was held about 2 mm above the center of a clean silicon surface. The silane evaporated from the drop and diffused radially while reacting with the silicon (Si/SiO_2) surface. The central part of the silicon surface, closest to the drop, became maximally hydrophobic, with the contact angle of water about 100°, whereas its peripheral zone remained wettable by water with a near-zero contact angle. In air, small drops (1 to 2 mm) of water move on such a surface radially outward with typical speeds of 0.2 to 0.3 cm/s. However, when saturated steam (100°C) condenses on such a surface, even smaller drops (0.1 to 0.3 mm) attain speeds (*9*) that are two orders of magnitude higher than those observed under ambient conditions (Fig. 1) (*10*).

How do the drops acquire such high speeds? A loss of interfacial resistance by a hydrodynamically lubricating water film on the surface could speed up drop motion, but on a nonwettable surface, where the contact angle is nonzero, a liquid film breaks up to produce numerous disconnected droplets. Previous studies (*11*) detected only a molecular or submolecular film of adsorbed water between condensed droplets, which are unlikely to provide substantial hydrodynamic lubrication to the moving drops.

Other plausible scenarios are that the wetting hysteresis is bypassed under rapid condensation and/or that additional energy is supplied to the drop to surmount hysteresis. We examine these scenarios in some detail. When a liquid drop is placed on a surface with an energy gradient, the Laplace pressure within the drop attempts to equilibrate quickly (*12*, *13*). Thus, the drop assumes the shape of a semispherical cap (*14*) to create nearly equal contact angles (θ_d) at edges A and B (Fig. 2). However, because θ_d is greater than the advancing contact angle at B (θ_{aB}), but less than the receding contact angle at A (θ_{rA}), the uncompensated wetting forces act at both A and B, which propel the whole drop toward the region of higher wettability. Typical speeds of such motion depend on the drop size and hysteresis but are in the range of a few millimeters per second. In the presence of fast condensation, however, the drop movement can be aided by the direct condensation of steam and by coalescence with other drops.

Let us consider the case of small drops, which do not move on the surface because of hysteresis but grow by the condensation of steam. Condensation causes the contact angles at A and B to surpass θ_{aA} and θ_{aB}. However, as the Laplace pressure attempts to equilibrate within the drop, the dynamic contact angles at A and B now assume an average value of θ_{aA} and θ_{aB}, which is greater than θ_{rA} but smaller than θ_{aA}. Thus, the contact line at A neither advances nor recedes. However, as the dynamic contact angle at B is greater than θ_{aB}, it moves toward the region of higher wettability. The characteristic velocity of B by condensation (*11*) is $V_1 \sim 2k_w\Delta T/(\rho HR)$, where k_w is the thermal conductivity, ρ is the density, H is the heat of vaporization of water, R is the base radius of the drop, and ΔT is the degree of subcooling of the substrate surface from that of steam. For drops from 0.1 to 0.3 mm, the drop edge moves with a velocity of about 20 to 40 μm/s and catches up and coalesces with other droplets condensing ahead of it. At a high rate of nucleation, the rate of coalescence can be so fast that edge B advances far more rapidly than

Department of Chemical Engineering, Lehigh University, Bethlehem, PA 18015, USA.

*To whom correspondence should be addressed.

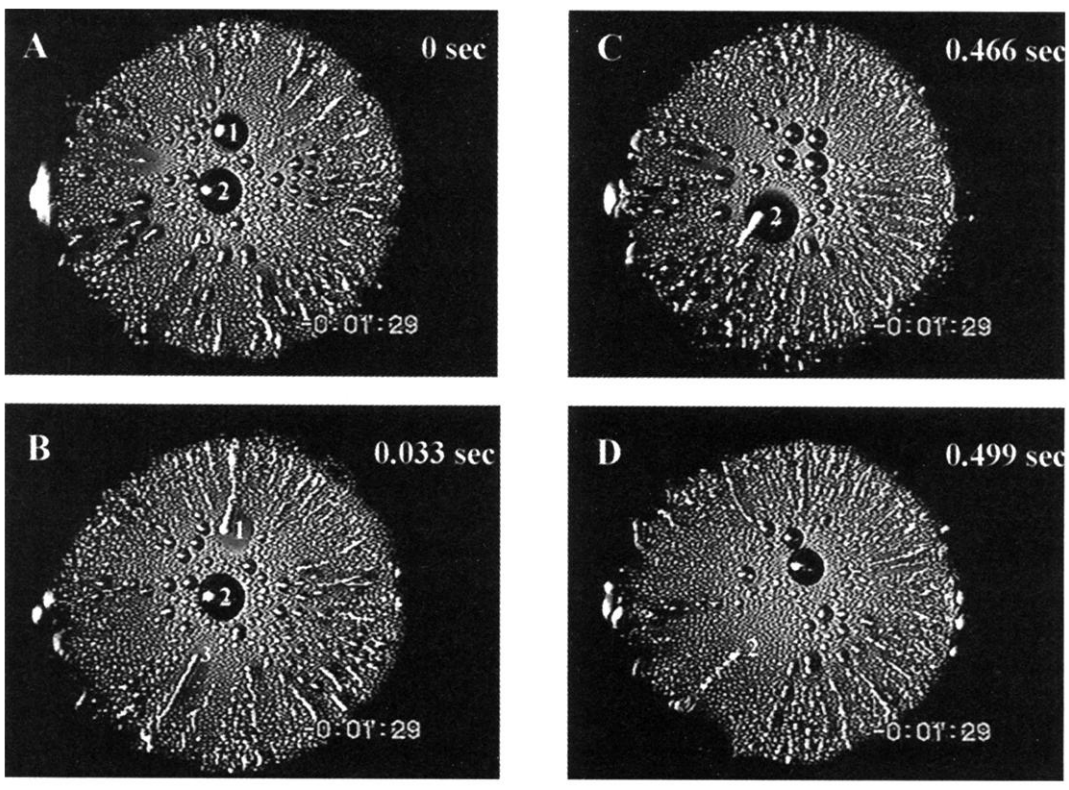

Fig. 1. Video prints showing fast movements of water drops (indicated by the plume- and streaklike appearances) resulting from the condensation of steam on a silicon wafer possessing a radial gradient (1 cm diameter) of surface energy. (**A**) and (**B**) show that drops 1 and 3 leave their original positions to cross the edge of the gradient in about 0.033 s. These movements leave behind streaklike appearances, which are due to the flashes of light reflecting from the drops during fast movements. The central drop (2) does not initially move, as it is on the weakest part of the gradient. However, after 0.47s, as the drop becomes off-centered, it rapidly crosses the gradient (**C** to **D**) zone.

V_1. θ_d at edge A thus continues to decrease until it becomes smaller than θ_{rA}, when the whole drop is dragged toward the more wettable part of the gradient.

A rough estimate of drop speeds (V) resulting from coalescence can be made by considering two drops of equal size of radii D coalescing with each other, in which the drop edges move by a net distance of ~0.37D. We consider a situation of low contact angle ($\theta \sim 45°$) so that the drop motion can be described approximately by lubrication theory (*15*). The energy budget of the process is the difference between the interfacial energies of the liquid drop before and after coalescence [$\sim 0.1\pi D^2\gamma f(\theta)$], where γ is the surface tension of the drop and $f(\theta) = (2-3\cos\theta + \cos^3\theta)/\sin^2\theta$. Considering that the time scale of coalescence $\tau = 0.37D/V$ is governed by the viscous drag forces at the contact line, the total energy dissipation is estimated to be $6\eta V^2 D\alpha\tau/\theta$, where η is the viscosity of the liquid and α is a logarithmic factor (~12) required to prevent divergence of shear stress at the contact line. Balancing of the two energies leads to the speed of coalescence approaching 1 m/s (*16*).

For saturated steam condensing on a gradient surface, these fast motions are biased toward the higher energy side of the gradient (*17*) and are facilitated by at least three factors. First, a drop always grows by condensation toward the more wettable part of the gradient and thus catches up with other drops condensing ahead of it. Second, the rate of nucleation increases with wettability; hence the probability of coalescence at edge B is higher than that at edge A (Fig. 2). Finally, as the drop starts moving, it grows in size by sweeping up other drops in its path and leaves behind a cleaner area for fresh condensation to begin. The drop gains more energy by coalescing with the larger drops ahead of it, not with the freshly nucleating drops behind it. The process thus autoaccelerates in order to produce a net movement of the drop toward the region of higher wettability.

The coupling between the surface tension gradient and the condensation of steam is evident in that the droplet speed slows down as soon as the steam flow is shut off (*18*). In the quiescent state, condensation continues at a slow rate and only slow motion of drops is observed. Occasionally, drops coalesce and the resultant drop moves toward the region of higher wettability (*19*). On a homogeneously hydrophobic substrate, the droplets grow and coalesce randomly. with the surrounding drops leading to a two-dimensional (2D) random walk (*20*). During the coalescence, however, drop edges retract with speeds comparable to the biased movements of condensing drops on a gradient surface.

Such coalescence-induced drop motion can be harnessed to enhance the performance of heat exchangers. In common heat exchangers, a metallic wall separates a cold water stream from a superheated vapor. Heat released from the condensation of steam is conducted through the metallic wall and transferred to the cold fluid. In practice, the heat flow is compromised by the thin insulating liquid film that accumulates on the steam side of the heat exchanger. Although various gravity-driven methods have been designed to remove the insulating water (*21*) from the surface of heat exchangers, there exists no good mechanism to remove water from the horizontal surfaces of heat exchangers and from those operating in microgravity situations. Here we describe a mechanism of water removal that takes advantage of the surface energy gradient.

Figure 3 provides the schematic of a heat exchanger made up of a cylindrical block (5 cm in diameter) of copper (*22*), the curved side of which is insulated with thick Teflon in order to ensure unidirectional (axial) heat conduction. The steam side of the copper block was prepared by polishing it to a mirror finish and then coating it with a thin film (~100 nm) of silicon by vacuum deposition. A radially outward gradient of octyltrichlorosilane was then formed on this surface by means of diffusion-controlled silanization. Saturated steam (100°C) was passed over the gradient surface, while the other end of the block was cooled by cold water. As the condensing drops are continually removed

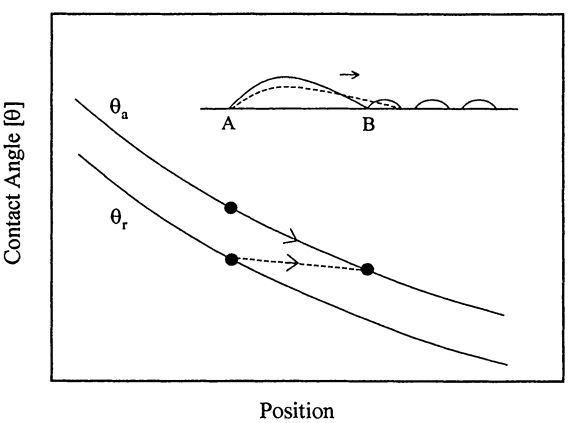

Fig. 2. Schematics of a 1D wettability gradient of a surface. θ_a and θ_r represent the advancing and receding contact angles, respectively. In the absence of hysteresis, the driving force for the drop motion is provided by the difference of the equilibrium contact angles at points at B and A. Hysteresis reduces the driving force (dotted arrow). The upper right inset shows that additional driving force can be gained from coalescence with other droplets, which nucleate and grow ahead of the main drop.

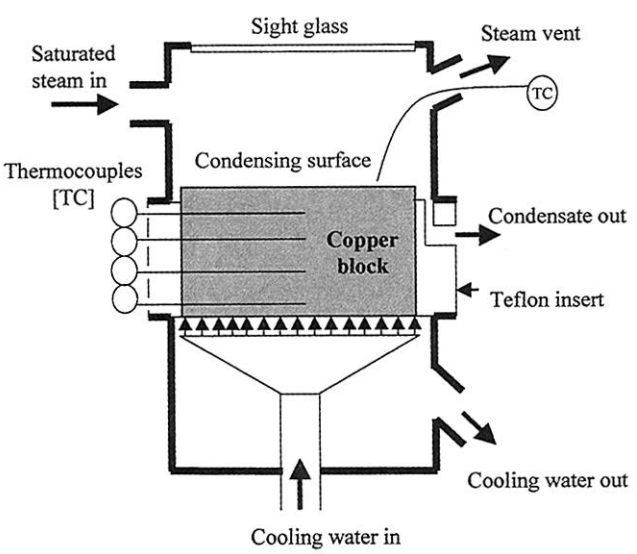

Fig. 3. Schematics of a heat exchanger. The heat flux (J_q) through the surface is estimated by knowing the conductivity (k_{cu}) of the copper block and the temperature gradient (dT/dy) as follows: $J_q = k_{cu}dT/dy$. The temperature gradient within the block was measured with four thermocouples inserted radially in different positions of the block, from which the temperature of the copper-steam interface (T_0) was extrapolated. The difference between T_0 and that of steam (T_s) gives the degree of subcooling of the surface.

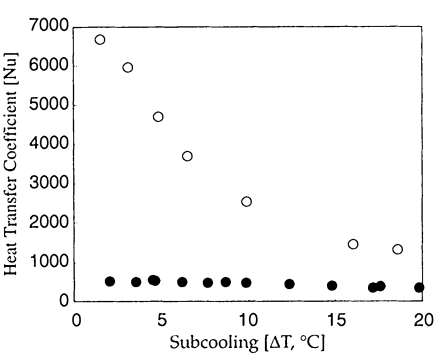

Fig. 4. The heat transfer coefficient of the copper block is enhanced with a chemical gradient. The heat transfer coefficient (Nu) is expressed in a dimensionless form as follows: $Nu = J_qD/(k_w\Delta T)$. Here, J_q is the heat flux, D is the diameter of the copper block, k_w is the conductivity of water, and ΔT is the degree of subcooling of the condensed liquid. The closed circles (●) correspond to a siliconized copper surface, where steam condenses as a thin film. The open circles (O) correspond to the gradient surface, where steam condenses into drops that are removed by the surface tension gradient.

by the surface tension gradient, the surface of the heat exchanger is renewed (*23*), thus enhancing heat flux through it. Figure 4 compares the heat transfer coefficients of the steam side of the heat exchanger under two situations: filmwise condensation on a horizontal unmodified surface and dropwise condensation on the gradient surface (*24*). The surface treatment enhances the heat transfer by a factor of 3 when the surface is subcooled (ΔT) from that of steam by about 20° and by a factor of 10 when subcooling is about 2°.

This methodology is also applicable on vertical surfaces, where the surface tension forces can be used in conjunction with gravity. This concept was demonstrated by preparing a 1D periodic gradient on a silicon wafer by diffusion-controlled silanization. Here the condensing drops are propelled from the hydrophobic zones and accumulate in the narrow hydrophilic channels to ultimately drain down because of gravity (*25*). A comparison has been made between such a drop removal mechanism and the usual method of promoting dropwise condensation by adding a surfactant (such as oleylamine) in the steam or hydrophobizing the surface by an organic coating (such as by silanization). Both the above methods yielded similar heat transfer coefficients [Nusselt number (Nu) ~ 1300], whereas the gradient surface under similar operating conditions exhibited a higher heat transfer coefficient (Nu = 2750). Clearly, surface tension forces can enhance the effectiveness not only of horizontal heat exchangers but of vertical heat exchangers as well. A heat exchanger surface possessing a periodic gradient has the additional advantage that its size can be scaled up in both horizontal and vertical directions without compromising the benefits of the gradient.

The phenomenon described here could also be useful in other types of heat transfer problems involving two-phase flow, an example of which is capillary force–driven thermosyphoning in heat pipes. A capillary force–driven heat pipe (*26*) consists of a closed container that has a heating and a cooling section. A fluid is thermally evaporated in the heating section, the vapor of which flows to the cooling section and condenses. The condensed fluid returns to the heating section by capillary action. The circulation of fluid and the corresponding heat transfer thus created within the heat pipe have a wide range of applications, including temperature stabilization in aerospace situations, thermosyphoning in Rankine engines, removal of heat from integrated microelectronic chips and controlled cooling of human body parts during cryogenic surgery. The standard way of pumping a fluid from the condensation to the evaporation section uses a wicking material, which is placed against the inner wall of the heat pipes. It is possible that the capillary pumping inside a heat pipe can be facilitated by designing a surface tension gradient in its inner wall.

References and Notes

1. D. Edwards, H. Brenner, D. Wasan, *Interfacial Transport Processes and Rheology* (Butterworth-Heinemann, Boston, 1991).
2. M. Grunze, *Science* **283**, 41 (1999).
3. M. A. Burns *et al.*, *Proc. Natl. Acad. Sci. U.S.A.* **93**, 5556 (1996).
4. B. S. Gallardo *et al.*, *Science* **283**, 57 (1999).
5. T. Ondarcuhu, M. Veyssie, *J. Phys. (Paris) II* **1**, 75 (1991).
6. M. K. Chaudhury, G. M. Whitesides, *Science* **256**, 1539 (1992).
7. K. Ichimura, S.-K. Oh, M. Nakagawa, *Science* **288**, 1624 (2000).
8. See Web Figs. 1 and 2 (*27*).
9. Visit http://www.lehigh.edu/~mkc4/movie1.mov to view the movements of water drops condensing on a radial gradient surface in real time.
10. Measurement of these speeds is limited by the resolution of the standard video setup, which allows us to estimate the highest speed as 15 cm/s. Some preliminary experiments using high-speed video indicate that some of the drops move at speeds as high as 1.5 m/s [see Web fig. 4 (*27*)].
11. A. Umur, P. Griffith, *J. Heat Transfer* **87**, 275 (1965).
12. H. P. Greenspan, *J. Fluid Mech.* **84**, 125 (1978).
13. F. Brochard, *Langmuir* **5**, 432 (1989).
14. This is true when the drop size is smaller than the Laplace length and the capillary number (Ca) is much less than unity. In our case, $Ca < 10^{-3}$.
15. P. G. De Gennes, *Rev. Mod. Phys.* **57**, 828 (1985).
16. This calculation overpredicts the droplet speed somewhat, because some of the surface energy is used up in the viscous mixing of drops. More detailed calculation shows that the droplet speed resulting from binary coalescence can easily reach about 50 cm/s. With multiple coalescence, drop speed can exceed the above values.
17. The movement of the drop edge could be facilitated by a thermal gradient of the drop close to the contact line. This is likely a second-order effect, because the fast drop motion is observed even when the substrate surface is subcooled by only about 2 K from the temperature of steam.
18. Visit http://www.lehigh.edu/~mkc4/movie2.mov to view the slowing down of droplet speeds as the steam is shut off.
19. H. Zhao and D. Beysens [*Langmuir* **11**, 627 (1995)] made similar observations in the context of the water vapor (~20°C) condensing on a slightly subcooled gradient surface.
20. Visit http://www.lehigh.edu/~mkc4/movie3.mov to view the random movement of liquid drops coalescing on a horizontal hydrophobic surface without a gradient.
21. A. Bejan, *Heat Transfer* (Wiley, New York, 1993).
22. G. Koch, D. C. Zhang, A. Leipertz, *Heat Mass Transfer* **32**, 149 (1997).
23. Visit http://www.lehigh.edu/~mkc4/movie4.mov to view the movements of a liquid drop on the steam side of a heat exchanger.
24. Here we performed all of the measurements at a very low steam velocity (~0.2 m/s) in order to minimize the effects produced by vapor shear. As is well known in the heat transfer literature and observed by us in preliminary experiments, greater heat transfer can be obtained by increasing the steam flow rate.
25. Visit http://www.lehigh.edu/~mkc4/movie5.mov to view the movements of drops within two channels of a 1D periodic gradient surface.
26. A. Faghri, *Heat Pipe Science and Technology* (Taylor & Francis, Washington, DC, 1995).
27. See www.sciencemag.org/cgi/content/full/291/5504/633/DC1 for details of the methods used to prepare the gradient surfaces and their characterizations.

28. Inspiring discussions with P. G. De Gennes, A. Sharma, and M. Shanahan are gratefully acknowledged. This work was funded by an NSF REU, Dow Corning, and Air Products.

26 September 2000; accepted 1 December 2000

Capture of a Single Molecule in a Nanocavity

Li-Qun Gu,[1]* Stephen Cheley,[1]* Hagan Bayley[1,2]†

We describe a heptameric protein pore that has been engineered to accommodate two different cyclodextrin adapters simultaneously within the lumen of a transmembrane β barrel. The volume between the adapters is a cavity of ~4400 cubic angstroms. Analysis of single-channel recordings reveals that individual charged organic molecules can be pulled into the cavity by an electrical potential. Once trapped, an organic molecule shuttles back and forth between the adapters for hundreds of milliseconds. Such self-assembling nanostructures are of interest for the fabrication of multianalyte sensors and could provide a means to control chemical reactions.

One way to create functional nanostructures is to modify existing biological structures, especially multisubunit proteins. For example, the F_1-adenosine triphosphate synthase (F_1-ATPase) motor has been used to rotate actin filaments (*1*) and inorganic "nanopropellers" (*2*). In our laboratory, a seven-subunit protein pore, staphylococcal α-hemolysin (αHL), has been modified, both noncovalently and covalently, to produce structures with a variety of properties. For example, when molecular adapters, such as cyclodextrins (CDs) (*3–6*) and cyclic peptides (*7*), are lodged within the lumen of the pore, they alter the magnitude and selectivity of ion conduction in a transmembrane potential. The adapters can also act as binding sites for guest molecules that block conduction by the pore (*3, 5, 7*). In addition, flexible polymers have been covalently tethered within the lu-

[1]Department of Medical Biochemistry and Genetics, Texas A&M University System Health Science Center, College Station, TX 77843, USA. [2]Department of Chemistry, Texas A&M University, College Station, TX 77843, USA.

*These authors contributed equally to this report.
†To whom correspondence should be addressed. E-mail: bayley@tamu.edu